Optical Materials 77 (2018) 48–54

Contents lists available at ScienceDirect

Optical Materials

journal homepage: www.elsevier.com/locate/optmat

Supramolecular nanodots derived from citric acid and beta-amines with high quantum yield and sensitive photoluminescence

Xianrui Meng [a, 1], Yunjing Wang [a, 1], Xiaohui Liu [a], Mengwei Wang [a], Yanshan Zhan [a], Yingqiu Liu [a], Weiwei Zhu [a], Wenkai Zhang [a, *], Lijuan Shi [b, **], Xiaomin Fang [a, ***]

[a] Institute of Functional Organic Molecular Engineering, Henan Engineering Laboratory of Flame-Retardant and Functional Materials, College of Chemistry and Chemical Engineering, Henan University, Kaifeng 475004, PR China
[b] Key Laboratory of Coal Science and Technology of Ministry of Education and Shanxi Province, Taiyuan University of Technology, Taiyuan 030024, PR China

ARTICLE INFO

Article history:
Received 12 September 2017
Received in revised form
1 January 2018
Accepted 4 January 2018

Keywords:
Carbon nanodots
Supramolecules
Photoluminescence
Exitation dependence
Sensitiviy

ABSTRACT

Herein, we reported the characterization of a highly fluorescent and sensitive amorphous nanodots synthesized by hydrothermal treatment of citric acid in the presence of various β-amines below 200 °C. Five-membered ring fused 2-pyridone compounds are effectively produced in the condensation reaction, and serve as the main building blocks to self-assemble into supramolecular nanodots under hydrogen bonding. The 2-pyridone compounds are not the sole blue species, but effectively enhance the photoluminescence quantum yield of citric acid derived nanodots. Compared with the excitation-independent emission in dilute solution, the dense nanodots exhibit red-shifted, suppressed and unexpected excitation-dependent emission. Moreover, the supramolecular nanodots have high sensitivity in various ambient conditions, such as pH, solvent polarity and metal ions.

1. Introduction

Photoluminescent carbon dots (CDs) are increasingly being explored as novel fluorescent nanomaterials due to their strong fluorescence, low cytotoxicity, excellent water solubility and stable photoluminescence, which make them great promising materials for applications in optoelectronic and energy devices, photocatalyst, sensor, and bioimaging [1–8]. Various approaches have been developed to fabricate CDs including “top-down” and “bottom-up” methods. The “top-down” methods refer to carving bulk carbon materials into nanoparticles by using physical or chemical approaches, such as acid oxidation, electrochemical, and hydrothermal. Compared with “top-down” routes, the “bottom-up” routes have obvious advantages in adjusting the composition and physical properties of CDs by the careful selection of diversified organic precursors and carbonization conditions via thermal pyrolysis or carbonization. In the recent years, citric acid (CA) has become one of the most frequently used bioproducts for the synthesis of CDs through bottom-up carbonization routes due to the direct process involved and high fluorescence quantum yields (QYs). Many CDs have been prepared from CA and amines via heating, hydrothermal methods or microwave assisted methods [9–18]. However, because of the complex constituent of the synthesized CDs and consequently their undetermined chemical structures, there are ongoing debates over the origins of their fluorescence [9,19–22]. Therefore, identifying the compositions and determining the related chemical structures are essential for resolving the fluorescence origins of citric acid derived carbon dots (CACDs). Lately, the possible origin of their luminescent properties has been revealed by isolation and identification of luminescent species from the CACDs. Detailed analyses confirmed the chemical structure as citric-acid derived organic molecules or fluorophores [11,21,23–25]. Yang's group [26] and Kasprzyk's group [27] have reported a series of five ring fused 2-pyridone based fluorophores from condensation of CA and specific amines.

However, the photoluminescence (PL) intensity and quantum yields of CACDs are diminished greatly as the pyrolysis of the CA-amine complex proceeds to the high temperature, because the strongly intense molecular fluorophore is gradually consumed as

* Corresponding author.
** Corresponding author.
*** Corresponding author.
E-mail addresses: zhangwenkai@henu.edu.cn (W. Zhang), shilijuan@tyut.edu.cn (L. Shi), xmfang@henu.edu.cn (X. Fang).
[1] These authors contributed equally to this work.

https://doi.org/10.1016/j.optmat.2018.01.005
0925-3467/

the building block of the much less photoluminescent carbogenic core [11,13,28,29]. Therefore, low temperature (mainly below 200 °C) during pyrolysis seems to be the key to preserve the fluorescence. Zhang et al. suggested that an intermediate form of self-assembled organic dots between carbon dots and fluorophores is dominant in the CACDs that are prepared through the condensation of CA and amines at low reaction temperatures [24]. Chan's group disclosed CA-derived nanodots exist as supramolecular clusters with their individual monomer units linked together through noncovalent bonding forces [30]. Recently, we performed a study of the formation mechanism of nanodots prepared from CA-amine system and demonstrated the self-assembly behaviors in the complex system [31]. It was found that a number of CA and a single diethylenetriamine (DETA) combined together via hydrogen bonding to fabricate self-assembled constructions, that was, DETA@5CA. Then the dimeric and trimeric fluorophores coupled with DETA@5CA led to "dots" topologies in the CNDs solution. However, this area is still in its infancy and faces several key challenges. First, more synthetic approaches should be developed to shed light on the role of 2-pyridone compounds in the fluorescence of CACDs. Second, the chemical structure and intermolecular force corresponding to these amorphous/molecular "dots" is difficult to be characterized, and the effect of self-assembly on PL of CACDs remains to be further investigated.

In this work, we described the structure and photoluminescence properties of the supramolecular nanodots that are formed by hydrothermal treatment of CA in the presence of various β-amines below 200 °C. Five-membered ring fused 2-pyridone compounds are effectively produced in the condensation reaction, and serve as the main building blocks to self-assemble to supramolecular nanodots under noncovalent bonding. In dilute solution, the 2-pyridone fluorophores are identified as the PL origin of nanodots, exhibiting high quantum yield and excitation-independent emission. While the concentrated nanodot solution gives red-shifted, suppressed and unexpected excitation-dependent PL. It was also found that CACDs have high sensitivity in various ambient conditions, such as pH, organic solvent and metal ions. In the present systems, molecular fluorophores bonded with supra-molecules are important PL and morphological origin, which is very different with previous sp [2]-carbon networks and surface defects.

2. Experimental section

2.1. Chemicals

Citric acid (CA), ethylenediamine (EDA), 1,2-propylenediamine (AP), diethylenetriamine (DETA), triethylenetriamine (TETA), tetraethylenepentamine (TEPA) and dimethylvinylenediamine (DMEDA) were purchased from Sigma-Aldrich. Ethanol and acetone were purchased from the Sinopharm Chemical Reagent Co., Ltd. The other reagents were analytical-grade.

2.2. Preparation of supramolecular nanodots

Nanodots were synthesized by a hydrothermal treatment of citric acid and various β-amines according to previous reports [15,16]. In a typical procedure, 0.42 g (2 mmol) of citric acid and 0.44 g (6 mmol) of 1,2-propylenediamine (AP) were dissolved into 15 mL water, and stirred to form a clear solution. The mixed solution was transferred to a 30 ml Teflon-equipped stainless-steel autoclave, and then heated to 180 °C and kept for additional 4 h. After that, the solution naturally cooled to room temperature. Next it was dried by rotary evaporation under reduced pressure, and then yellow viscous oil was obtained. Then the oil was rinsed with acetone, followed by supersonic expansion and centrifugation at 10,000 rpm for 0.5 h. The precipitated material at the bottom of the centrifuge was vacuum dried at 65 °C and the brown powder was denoted as Dots-AP. Similarly, Dots-EDA, Dots-DETA, Dots-TETA, Dots-TEPA and Dots-DMEDA were prepared by using ethylenediamine (EDA), diethylenetriamine (DETA), triethylenetetramine (TETA), tetraethylenepentamine (TEPA) and N,N′-dimethylethylenediamine (DMEDA) as β-amines, respectively.

2.3. Characterization

The atomic force microscope (AFM) images were measured with Dimension Icon (Bruker Instruments Inc.) on new cleaved mica surface in tapping mode in air. High resolution microscopy measurements were performed using a JEM1200EX transmission electron microscopy (TEM) with an operating voltage of 120 kV. X-ray photoelectron spectra (XPS) was performed on a Thermo Fisher Scientific ESCALAB 250XI photoelectron spectrometer with Al Kα ($h\nu = 1486.6$ eV) as the X-ray source. Fourier transform infrared spectroscopy (FT-IR) characterization was carried out on a Bruker Vertex 70 FTIR spectrometer. UV–vis absorption spectra were recorded with a Hitachi U4100 Spectrometer. A high-resolution electrospray ionization-mass spectrometry (ESI-MS) was performed on a Solarix XR FTICR (Fourier transform ion cyclotron resonance) mass spectrometer equipped with a 7.0 T magnet (Bruker Daltonics, Billerica, MA, USA). The PL spectra were recorded by a Hitachi F-7000 spectrophotometer, and the relative quantum yield (QY) of the CDs were measured via the slope method by using quinine sulfate (in 0.5 M H_2SO_4, $\Phi = 0.54$) as a reference. For details in the mathematic calculation of quantum yields, please refer to the Supporting Information. The time-resolved PL spectra were performed with F980 spectrometer (Edinburgh Instruments, UK), equipped with a single photon photomultiplier detector (S900-R). The pulse width, wavelength, and repetition rate were chosen as 40 ps, 360 nm, and 5 MHz, respectively.

3. Results and discussion

3.1. Morphological and chemical structure of nanodots

The synthetic approach for supramolecular nanodots follows the hydrothermal treatment of citric acid in the presence of β-amines, including EDA, AP, DETA, TETA, TEPA and DMEDA. In this process, hydrothermal temperature is the key to preserve the fluorescence intensity of nanodots, because molecular fluorophores have been suggested to be dominant in the nanodots at low hydrothermal temperatures (mainly below 200 °C). Further carbonization occurs at higher temperatures, leading to the production of "carbon" rather than molecular nanodots. As shown in Fig. 1, a group of "dots" are detectable from atomic force microscope (AFM) image, giving the evaluated height of 0.8–1.5 nm for all nanodots. In addition to "dots", a wide range of morphologies can be also found in the products, such as worms (Fig. S1). Due to the little mass-thickness contrast of supra-molecular assemblies, almost none of carbogenic domains can be found in the TEM images (Fig. S2).

The element analysis (Table S1) and XPS (Fig. S3, Table S2) were performed to determine the chemical composition of nanodots. The high resolution N1s spectrum of the nanodots can be fitted into two broad peaks, where the peaks near 399 and 401 eV are likely to correspond to the pyridinic N and amide N respectively (Table S3), indicating the possible existence of pyridone compounds. Compared with the primary amine, the secondary amine is unlikely to form pyridone compounds, revealed by the low content of N atoms and the lack of pyridinic N in Dots-DMEDA. The C1s spectra can be fitted into 3 Gaussian peaks at 284.5, 286.1 and 288.6 eV

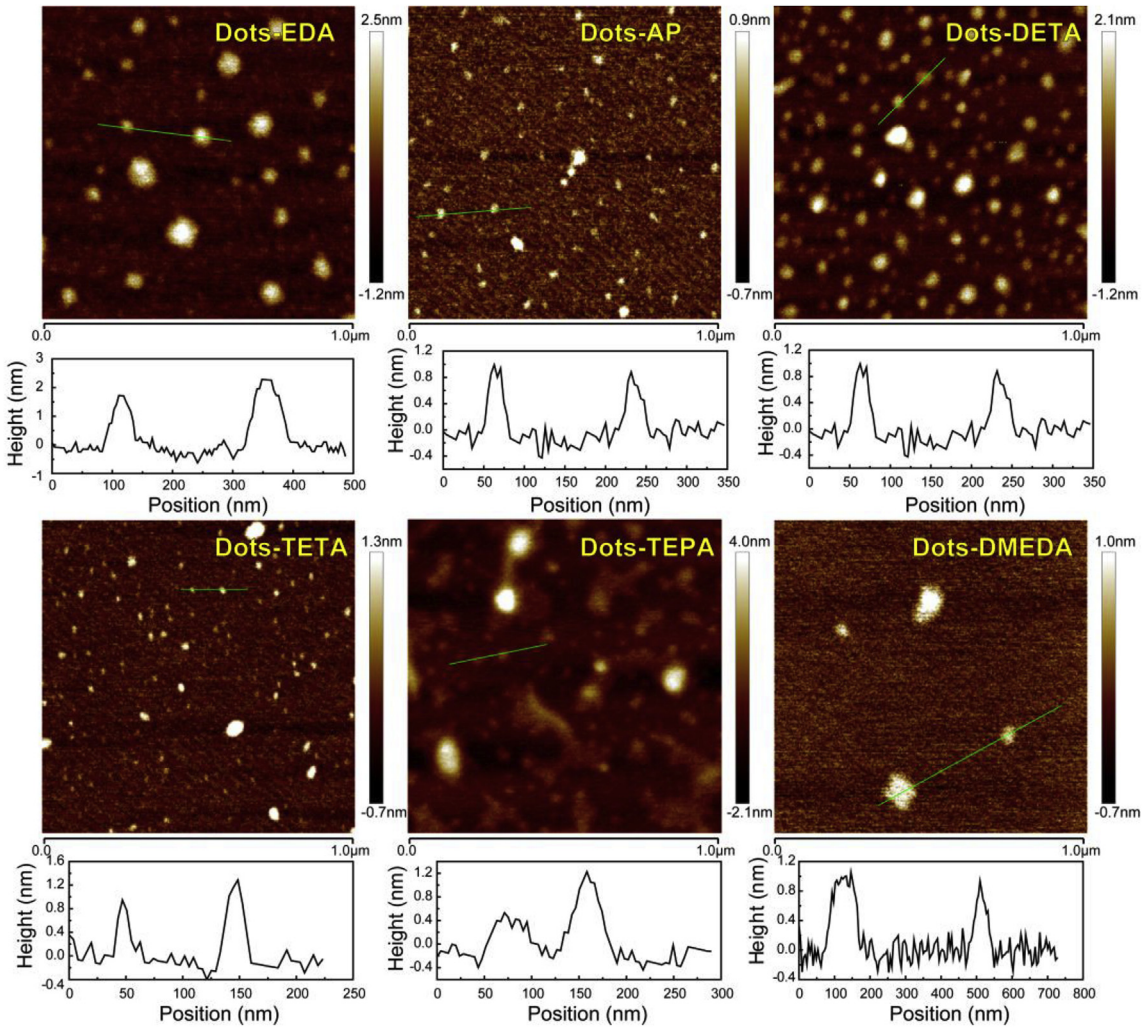

Fig. 1. AFM images of nanodots produced from the hydrothermal treatment of CA in the presence of various β-amines. Height profiles along lines show below.

(Table S4), which correspond to the aliphatic carbon (C—C/C = C), the C—N and the C = O in nanodots. The FTIR spectra of nanodots (Fig. S4) confirm the presence of amide functional groups, as evidenced by the C = O stretching vibration absorption peak (amide I band) near 1650 cm^{-1}, the N—H in-plane bending vibration absorption peak (amide II band) near 1570 cm^{-1}, and the C—N stretching vibration absorption peak (amide III band) near 1400 cm^{-1}.

High accuracy MS analyses of Dots-AP show the presence of an ion with $m/z = 195.1850$ (Fig. 2a), which correlates to the molecular formula of $C_9H_{11}N_2O_3^+$. The molecular structure is quite consistent with 2-methyl-5-oxo-1,2,3,5-tetrahydroimidazo[1,2-*a*]pyridine-7-carboxylic acid (named as **MeOIP**). According to previous reports [26,27], the formation mechanism of 2-pyridone compound consists of the formulation of an amide bond between CA and β-amine and several intramolecular condensation steps (Fig. S5). Another five nanodots were also characterized by high-resolution MS analyses (Fig. S6). The ions also match the chemical structure of proposed 2-pyridone compounds (Table S5) except for Dots-DMEDA. Thus we confirm that five-membered ring fused 2-pyridone compounds, including 5-oxo-1,2,3,5-tetrahydroimidazo[1,2-*a*]pyridine-7-carboxylic acid (**OIP**), 1-(2-aminoethyl)-5-oxo-1,2,3,5-tetrahydroimidazo[1,2-*a*]pyridine-7-carboxylic acid (**AEOIP**), 1-(2-((2-aminoethyl)amino)ethyl)-5-oxo-1,2,3,5-tetrahydroimidazo[1,2-*a*]pyridine-7-carboxylic acid (**BAEOIP**) and 1-(2-((2-((2-aminoethyl)amino)ethyl)amino)ethyl)-5-oxo-1,2,3,5-tetrahydroimidazo[1,2-*a*]pyridine-7-carboxylic acid (**TAEOIP**), can be easily fabricated through condensation reaction of CA with EDA, DETA, TETA and TEPA, respectively (Fig. 2b). However, the 2-pyridone compounds cannot be found in Dots-DMEDA, thus implying the formation mechanism of the compounds consists of several intramolecular condensation steps between CA and primary amines.

In addition, the trimers at m/z 275, 293, 315 and 333 ($z = 2$) are observed among the successive ion peaks in the MS spectra of Dots-AP (Table 1), all of which tend to produce a fragment ion of the protonated monomer at m/z 195 ($z = 1$), suggesting that the Dots-AP exist as supramolecular clusters in the aqueous phase, and the monomer of 195 Da is certainly the repeating unit of the clusters in the Dots-AP. Our proposal is supported by literature evidence [24,30,31]. Chan et al. claimed that the nitrogen and sulfur co-doped carbon nanoparticles exist as supramolecular clusters with their individual monomer units linked together through non-covalent bonding forces [30]. Since the 2-pyridone compounds are functionalized by carboxylic acid and amino groups, we believe that each nanodot exists as noncovalent supramolecular clusters in the aqueous phase with their monomer units linked together by a combination of ionic bonds and hydrogen bonds [31–34].

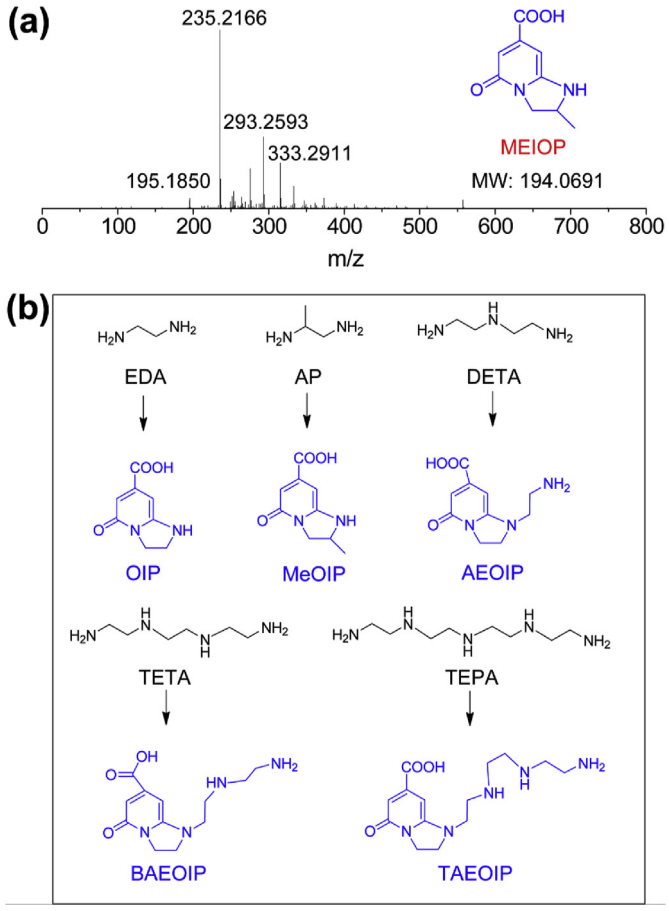

Fig. 2. (a) High resolution mass spectra of Dots-AP, indicating the presence of 2-pyridone compounds MeOIP. (b) Formation of 2-pyridone compounds from CA and various β-substituted amines.

Table 1
High resolution mass spectra indicating the presence of 2-pyridone compounds **MeOIP** and its supra-molecules.

m/z	Species
195.1850	MeOIP+H+
235.2166	MeOIP+H_2O+Na^+
251.1502	MeOIP+AP-H_2O+H^+
275.2484	(3MeOIP-2H_2O+2H)$^{2+}$
293.2593	(3MeOIP+2H)$^{2+}$
315.2803	(3MeOIP+2Na^+)$^{2+}$
333.2911	(3MeOIP+2H_2O+2Na)$^{2+}$

3.2. PL properties of nanodots

We therefore now describe the PL spectra conducted with as synthesized nanodots to understand the fundamental structure-property relationships for the so-called supramolecular nanodots. The absorption spectra in Fig. 3a display two peaks around 240 and 350 nm (220 and 320 nm for Dots-DMEDA), the former of which is ascribed to the π-π* transition of the nitrogen heterocyclic sp [2] domain and the latter to the n-π* transition of the carbonyl bond [35]. The PL emission spectra show maximum intensity at $\lambda_{em} = 440$ nm, and the PL excitation spectra show two peaks at $\lambda_{ex1} = 240$ nm and $\lambda_{ex2} = 355$ nm, which is coincident with the π-π* and n-π* transition, respectively (Fig. 3b and c). Although the N-substitutional groups on five-membered ring of 2-pyridone compounds are quite different, even that pyridone structures are not formed in Dots-DMEDA, all the nanodots show no significant difference in PL spectra. Thus, the blue species is not exclusive to 2-pyridone compounds in CA derived nanodots. Dong et al. reported the blue emission of carbon dots with $\lambda_{ex} = 360$ nm and $\lambda_{em} = 460$ nm, which are prepared by pyrolysis of CA at 200 °C in the absence of amine [18], indicating the blue emissive fluorophore may be also formed by condensation reaction between CA molecules. However, the PL quantum yields (QYs) of CA based nanodots are strongly dependent on the nitrogen contents (Fig. 3d). The PLQY of carbon dots reported by Dong et al. is only 9.0% (without N), while the PLQY enhances for all nitrogen containing nanodots ranging from 11% to 74%.

2D PL excitation (PLE) contour map in Fig. 4a reveals two discrete and relatively narrow luminescence maximums for dilute Dots-AP aqueous solution (0.01 mg/mL), that is, excitation-independent emission. The PL decay curve of Dots-AP is well explained by monoexponential decay functions, yielding a lifetime of 13.6 ns (Fig. S7), indicating the PL originates from a single emissive species, that is, the fluorophore MeOIP. However, it is interesting the concentrated Dots-AP solution (1 mg/mL) shows three areas in 2D PLE map, two of which (labeled as I) are symmetric, but newly created asymmetric area (II) is asymmetric, giving the well-known excitation-dependent PL (Fig. 4b). The PL of Dots-AP shows redshift and emission intensities decrease when sample concentration increases from 10^{-6} mg/mL to 1 mg/mL, indicating the formation of excimer (Fig. S8). As the λ_{ex} increases from 200 to 400 nm, the PL emission peak of concentrated solution shows nearly no shift, however, the PL emission peak increases linearly with the increasing excitation wavelength as $\lambda_{ex} > 400$ nm, giving a slope of 0.45 (Fig. 4c). We also note that long wavelength emission at ~550 nm shows excitation peaks at 488, 362 and 240 nm, and the PL excitation spectra of concentrated solution largely overlap with the emission spectra ($\lambda_{em} = 440$ nm) of dilute solution (Fig. 4d), indicating long wavelength emission is clearly associated with the single fluorophore. To explain such red shift in the photoluminescence of nanodots, a model based on photon reabsorptions is suggested [36]. Since the Dots-AP exist as non-covalent supramolecular clusters of 2-pyridone monomer units, dimeric, trimeric and even bigger oligomeric aggregates are likely to be successively excited by increasing wavelength of light. First, an incoming photon with energy of $h\nu_0$ is absorbed by a smaller cluster in the solution and after a delay (lifetime), this excited oligomer emits a second photon with smaller energy of $h\nu_I$ due to Stokes shift. This photon is then absorbed by a bigger cluster in the solution; after a similar delay this cluster emits a third photon with even smaller energy of $h\nu_{II}$, and this photon will escape from the solution and contribute to the measured PL. The frequent occurrence of photon reabsorption results in a decrease in emission of the smaller clusters and an increase in emission of the larger ones. The denser the solution, the stronger the photon reabsorption, accordingly there will be more contribution to the total PL by larger clusters (with smaller energy gaps); as a result, the total PL will be shifted to red as the nanodot concentration is improved. After absorption of the photon emitted by the smaller cluster, the excited bigger cluster can relax its energy through two channels: radiative and nonradiative transitions. The energy will be transformed into thermal energy if the nonradiative relaxation channel is taken. On the other hand, as a result of Stokes shift, the photon emitted by the bigger cluster has lower energy than the photon emitted by the smaller cluster. Both the two factors combined together lead to the decrease in PL intensity in a concentrated solution compared with a dilute solution.

Many researches revealed that the photophysical properties can be tuned by external factors such as temperature, light and pH in the many molecular self-assembly systems which are mainly

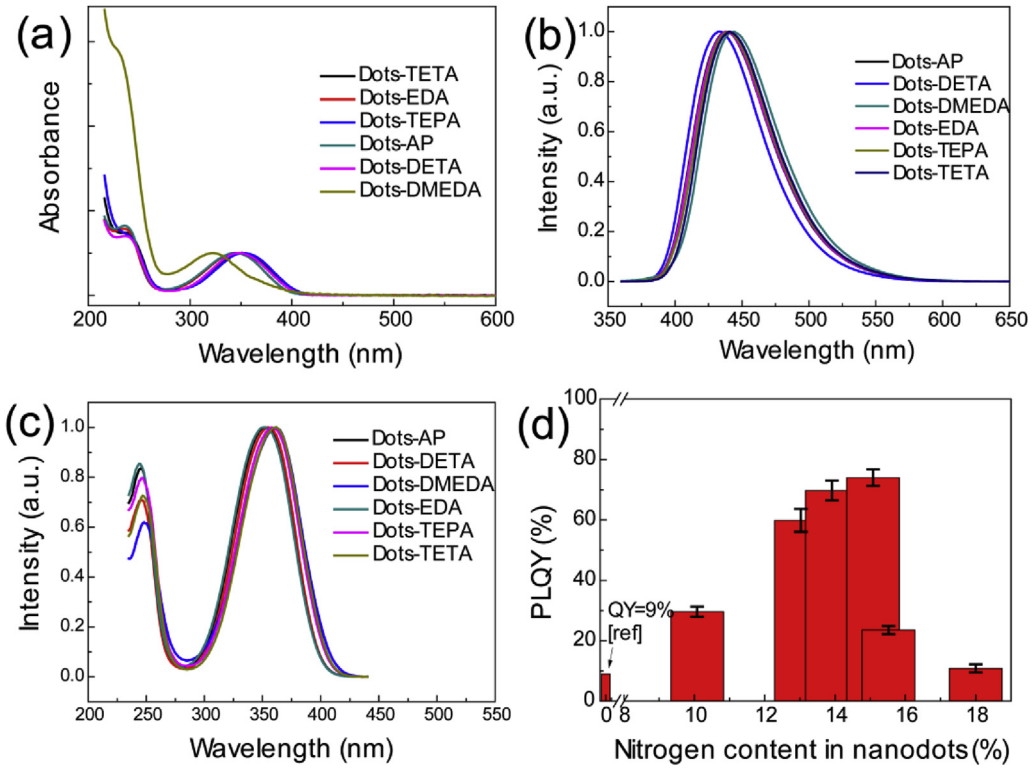

Fig. 3. (a) Absorption spectra. (b) PL emission spectra. (c) PL excitation spectra. (d) Photoluminescence quantum yields (PLQY) as a function of nitrogen contents. The nitrogen contents are determined by element analysis (Table S1).

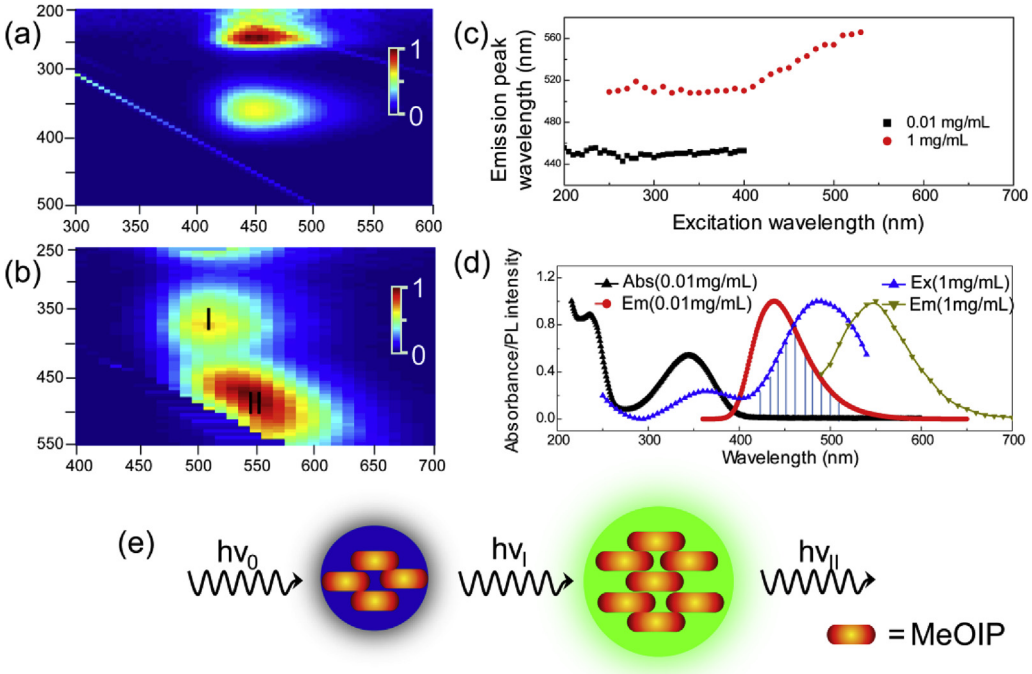

Fig. 4. (a) 2D PLE maps of Dots-AP solutions at a concentration of 10^{-2} mg/ml (a) and 1 mg/ml (b). (c) The PL intensity maximum positions as a function of excitation wavelength for dilute (black cube) and concentrated (red circle) solution. (d) The absorption, PL excitation and emission spectra of the dilute and concentrated solution. (e) Schematic diagram depicting the photon reabsorption processes: a smaller nanodot absorbs an incoming excitation photon with energy of $h\nu_0$ followed by subsequent emission of another photon ($h\nu_I$), which is then absorbed by a bigger nanodot, and finally this big nanodot emits an outgoing photon ($h\nu_{II}$). (For interpretation of the references to colour in this figure legend, the reader is referred to the Web version of this article.)

governed by hydrogen bonding interactions. These give us a hint that the supramolecular interactions in these supramolecular nanodots can be much favorable in sensing applications [37,38]. As seen in Fig. 5a, the emission intensity decrease in a solution of high

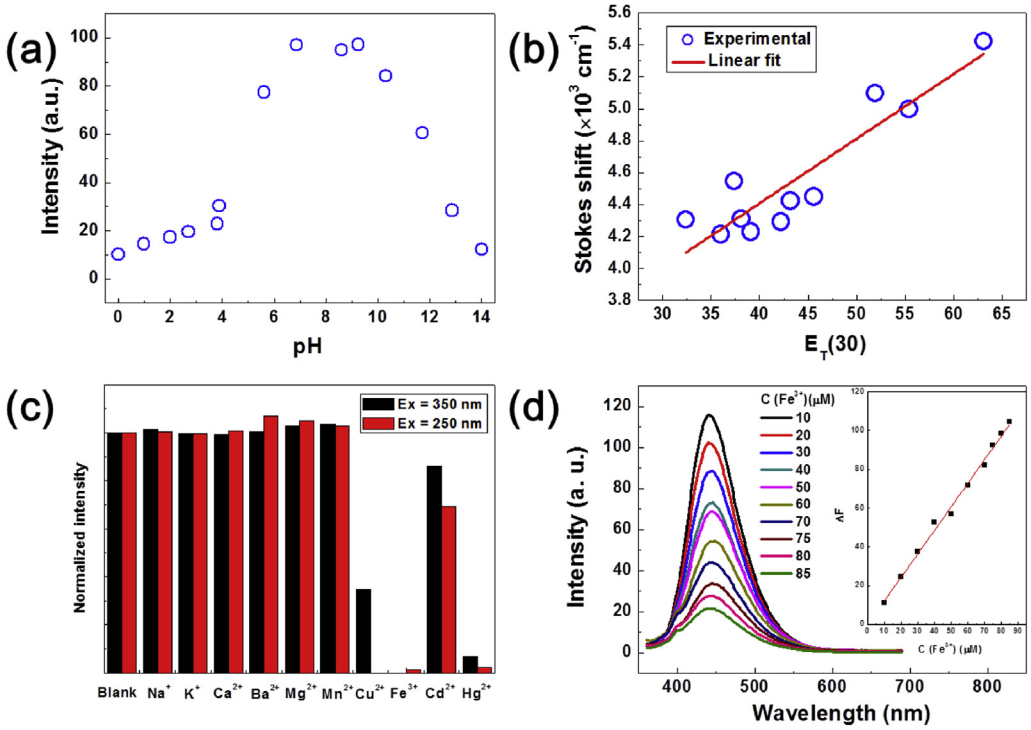

Fig. 5. (a) The effect of pH (a), solvent (b) and metal ions (c) on the fluorescence intensities of Dots-AP. (d) Typical PL quenching of Dots-AP in the presence of Fe^{3+} ions. Inset: the curve of the fluorescence quenching values (ΔF) vs. Fe^{3+} concentration in the range from 10 μM to 100 μM. $\Delta F = F_0 - F$, F_0 and F are the fluorescence intensities of Dots-AP at 450 nm in the absence and presence of Fe^{3+}, respectively.

or low pH. The pH dependent fluorescence can be understood in terms of extensive protonation-deprotonation of the amide groups given that the deprotonated amide groups have high electron-donating efficiency [39,40]. Owing to the intrinsic polarity, the dots are dispersible in many hydrophilic solvents with the solubility in the order of $H_2O > CH_3OH > C_2H_5OH >$ DMSO ≈ DMF > CH_3COCH_3 ≈ THF. Their Stokes shifts respond with near linearity to $E_T(30)$ [41], a measure of microscopic solvent polarity (Fig. S9, Fig. 5b). Proton transfer appears to control the excited state properties of fluorophore since there is discontinuity in Stokes shift as a function of protic versus aprotic solvents. Nanodots also exhibit high selectivity and specificity towards metal ions owing to their strong coordination interaction with amino groups, making them functional materials for sensitive and selective detection of metal ions. Due to the high sensitivity and selectivity, carbon nanodots have been used as a fluorescent probe for the detection of metal ions [42–44]. The fluorescence intensity ratios (F/F_0) of Dots-AP (50 μg/mL) were analyzed upon adding different metal ions (such as Na^+, K^+, Ca^{2+}, Ba^{2+}, Mg^{2+}, Mn^{2+}, Cu^{2+}, Fe^{3+}, Cd^{2+}, Hg^{2+}) to the sensing system. As shown in Fig. 5c, Fe^{3+} and Hg^{2+} produce significant quenching effect on the fluorescence of Dots-AP. We also find the excitation wavelength would affect the sensitivity and selectivity, revealed by the increasing quenching efficiency of Cu^{2+} by using 250 nm instead of 350 nm excitation light. Then, we explored the feasibility of using Dots-AP as fluorescent probes for the detection of Fe^{3+}. When Fe^{3+} with increasing concentration is added to the as-prepared Dots-AP solution, the fluorescence intensity of Dots-AP at 450 nm gradually decreases (Fig. 5d). The fluorescent quenching value ΔF has a good linear relationship with the concentration of Fe^{3+} in the range of 10–85 μM. When Fe^{3+} ions are added into the Dots-AP solution, they can coordinate with the —COOH and —NH in the MeOIP fluorophore, leading to significant fluorescence quenching [43,44].

4. Conclusions

In summary, we have adopted a one-pot hydrothermal approach to produce highly blue fluorescent supramolecular nanodots by the reaction of citric acid with beta-amines at relatively low temperature. The relationship between the supramolecular structure and morphology of “dots” is analyzed, and the physical model is proposed. A series of five-membered ring fused 2-pyridone compounds are isolated from the as-prepared nanodots. The individual fluorophore monomer units link together through hydrogen bonding forces to produce dimer, trimer, etc. Thus, we suggest that the supramolecular cluster of 2-pyridone compounds lead to “dots” topologies in the nanodots solution under noncovalent bonding. The supramolecular nanodots exhibit high as well as nitrogen contents dependent fluorescence quantum yield in aqueous solution. In dilute solution, the supramolecular nanodots exhibit excitation-independent emission spectra, but the concentrated solution presents red-shifted, suppressed and unexpected excitation-dependent PL due to photon reabsorption. It is also found that CACDs have high sensitivity in various ambient conditions, such as pH, organic solvent and metal ions. Due to the high selectivity and sensitivity of CACDs to Fe^{3+}, the as-prepared CACDs can be used for quantitative detection of Fe^{3+} in aqueous solution. In the present systems, molecular fluorophores bonded with supramolecules are important PL and morphological origin, which is very different with previous carbogenic ones.

Acknowledgements

This work was supported by the National Natural Science Foundation of China (51403051; 21502042; 21403127; 21403151), Key Project of the Education Department of Henan Province (16A150003) and the Science and Technology Development Program of Henan Province of China (162102210023; 142300410122).

Appendix A. Supplementary data

Supplementary data related to this article can be found at https://doi.org/10.1016/j.optmat.2018.01.005.

References

[1] X. Wang, G. Sun, N. Li, P. Chen, Chem. Soc. Rev. 45 (2016) 2239.
[2] X. Li, M. Rui, J. Song, Z. Shen, H. Zeng, Adv. Funct. Mater. 25 (2015) 4929.
[3] A. Zhao, Z. Chen, C. Zhao, N. Gao, J. Ren, X. Qu, Carbon 85 (2015) 309.
[4] V. Georgakilas, J.A. Perman, J. Tucek, R. Zboril, Chem. Rev. 115 (2015) 4744.
[5] P. Miao, K. Han, Y. Tang, B. Wang, T. Lin, W. Cheng, Nanoscale 7 (2015) 1586.
[6] C. Ding, A. Zhu, Y. Tian, Acc. Chem. Res. 47 (2014) 20.
[7] Y. Wang, A. Hu, J. Mater. Chem. C 2 (2014) 6921.
[8] K. Hola, Y. Zhang, Y. Wang, E.P. Giannelis, R. Zboril, A.L. Rogach, Nano Today 9 (2014) 590.
[9] N. Dhenadhayalan, K.C. Lin, R. Suresh, P. Ramamurthy, J. Phys. Chem. C 120 (2016) 1252.
[10] S.J. Zhu, X.H. Zhao, Y.B. Song, S.Y. Lu, B. Yang, Nano Today 11 (2016) 128.
[11] L. Shi, J.H. Yang, H.B. Zeng, Y.M. Chen, S.C. Yang, C. Wu, H. Zeng, O. Yoshihito, Q. Zhang, Nanoscale 8 (2016) 14374.
[12] Y. Zhang, X. Liu, Y. Fan, X. Guo, L. Zhou, Y. Lv, J. Lin, Nanoscale 8 (2016) 15281.
[13] J. Huang, M.Z. Rong, M.Q. Zhang, Phys. Chem. Chem. Phys. 18 (2016) 4800.
[14] Y.P. Hu, J. Yang, J.W. Tian, J.S. Yu, J. Mater. Chem. B 3 (2015) 5608.
[15] D. Qu, M. Zheng, L. Zhang, H. Zhao, Z. Xie, X. Jing, R.E. Haddad, H. Fan, Z. Sun, Sci. Rep. 4 (2014) 5291.
[16] X. Li, S. Zhang, S.A. Kulinich, Y. Liu, H. Zeng, Sci. Rep. 4 (2014) 4971.
[17] Y. Dong, H. Pang, H.B. Yang, C. Guo, J. Shao, Y. Chi, C.M. Li, T. Yu, Angew. Chem. Int. Ed. 52 (2013) 7800.
[18] Y. Dong, J. Shao, C. Chen, H. Li, R. Wang, Y. Chi, X. Lin, G. Chen, Carbon 50 (2012) 4738.
[19] V. Strauss, J.T. Margraf, C. Dolle, B. Butz, T.J. Nacken, J. Walter, W. Bauer, W. Peukert, E. Spiecker, T. Clark, D.M. Guldi, J. Am. Chem. Soc. 136 (2014) 17308.
[20] S. Ghosh, A.M. Chizhik, N. Karedla, M.O. Dekaliuk, I. Gregor, H. Schuhmann, M. Seibt, K. Bodensiek, I.A.T. Schaap, O. Schulz, A.P. Demchenko, J. Enderlein, A.I. Chizhik, Nano Lett. 14 (2014) 5656.
[21] Y. Song, S. Zhu, S. Zhang, Y. Fu, L. Wang, X. Zhao, B. Yang, J. Mater. Chem. C 3 (2015) 5976.
[22] S. Wang, Z. Chen, I. Cole, Q. Li, Carbon 82 (2015) 304.
[23] W. Kasprzyk, S. Bednarz, P. Zmudzki, M. Galica, D. Bogdal, RSC Adv. 5 (2015) 34795.
[24] J. Zhang, L. Yang, Y. Yuan, J. Jiang, S. Yu, Chem. Mater. 28 (2016) 4367.
[25] H. Peng, Y. Li, C. Jiang, C. Luo, R. Qi, R. Huang, C. Duan, J. Travas-Sejdic, Carbon 100 (2016) 386.
[26] a) Y. Song, S. Zhu, S. Zhang, Y. Fu, L. Wang, X. Zhao, B. Yang, J. Mater. Chem. C 3 (2015) 5976;
b) S. Zhu, X. Zhao, Y. Song, S. Lu, B. Yang, Nano Today 11 (2016) 128.
[27] W. Kasprzyk, S. Bednarz, P. Żmudzki, M. Galica, D. Bogdał, RSC Adv. 5 (2015) 34795.
[28] M.J. Krysmann, A. Kelarakis, P. Dallas, E.P. Giannelis, J. Am. Chem. Soc. 134 (2012) 747.
[29] S. Hu, A. Trinchi, P. Atkin, I. Cole, Angew. Chem. Int. Ed. 54 (2015) 2970.
[30] Q. Hu, X. Meng, W. Chan, Anal. Bioanal. Chem. 408 (2016) 5347.
[31] (a) W. Zhang, L. Shi, Y. Liu, X. Meng, H. Xu, Y. Xu, B. Liu, X. Fang, H. Li, T. Ding, RSC Adv. 7 (2017) 20345;
(b) X. Liu, H.B. Li, L. Shi, X. Meng, Y. Wang, X. Chen, H. Xu, W. Zhang, X. Fang, T. Ding, J. Mater. Chem. C 5 (2017) 10302.
[32] L. Shi, N. Sun, L. Zheng, Chem. Commun. 51 (2015) 15700.
[33] C. Zhou, X. Cheng, O. Zhao, S. Liu, C. Liu, J. Wang, J. Huang, Soft Matt. 10 (2014) 8023.
[34] L. Shi, P. Sun, L. Zheng, Soft Matt. 12 (2016) 8682.
[35] F. Wang, Z. Xie, B. Zhang, Y. Liu, W. Yang, C. Liu, Nanoscale 6 (2014) 3818.
[36] (a) W. Zhang, D. Dai, X. Chen, X. Guo, J. Fan, Appl. Phys. Lett. 104 (2014), 091902;
(b) W. Zhang, Y. Wang, X. Liu, X. Meng, H. Xu, Y. Xu, B. Liu, X. Fang, H.B. Li, T. Ding, Phys. Chem. Chem. Phys. 19 (2017), 28653.
[37] X.T. Zheng, A. Ananthanarayanan, K.Q. Luo, P. Chen, Small 11 (2015) 1620.
[38] H. Nie, M. Li, Q. Li, S. Liang, Y. Tan, L. Sheng, W. Shi, S.X. Zhang, Chem. Mater. 26 (2014) 3104.
[39] T. Beppu, K. Tomiguchi, A. Masuhara, Y. Pu, H. Katagiri, Angew. Chem. Int. Ed. 54 (2015) 7332.
[40] W. Zhang, Y. Liu, X. Meng, T. Ding, Y. Xu, H. Xu, Y. Ren, B. Liu, J. Huang, J. Yang, X. Fang, Phys. Chem. Chem. Phys. 17 (2015) 22361.
[41] C. Reichardt, Chem. Rev. 94 (1994) 2319.
[42] F.R. Baptista, S.A. Belhout, S. Giordani, S.J. Quinn, Chem. Soc. Rev. 44 (2015) 4433.
[43] M. Zhou, Z.L. Zhou, A.H. Gong, Y. Zhang, Q.J. Li, Talanta 143 (2015) 107–113.
[44] S. Li, Y. Li, J. Cao, J. Zhu, L. Fan, X. Li, Anal. Chem. 86 (2014) 10201–10207.